Kobe University Repository : Kernel

PDF issue: 2026-11-03

Golf ball-like polymer particles with site-selective functionalization of concave and convex regions

Morishita, Takahiro ; Furukawa, Rintaro ; Matsumoto, Takuya ; Suzuki, Nozomu ; Suzuki, Toyoko ; Minami, Hideto

(Citation)
Reactive and Functional Polymers,227:106861

(Issue Date)
2026-10

(Resource Type)
journal article

(Version)
Version of Record

(Rights)
© 2026 The Authors. Published by Elsevier B.V.
This is an open access article under the Creative Commons Attribution-NonCommercial 4.0 International license

(URL)
https://hdl.handle.net/20.500.14094/0100505082

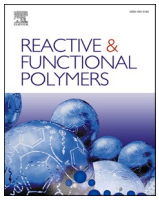
Reactive and Functional Polymers 227 (2026) 106861



Contents lists available at ScienceDirect

Reactive and Functional Polymers

journal homepage: www.elsevier.com/locate/react





Golf ball-like polymer particles with site-selective functionalization of concave and convex regions

Takahiro Morishita, Rintaro Furukawa, Takuya Matsumoto, Nozomu Suzuki, Toyoko Suzuki, Hideto Minami *

Department of Chemical Science and Engineering, Graduate School of Engineering, Kobe University, 1-1 Rokko, Nada-ku, Kobe 657-8501, Japan

ARTICLE INFO

Keywords:
Golf ball-like shape
Polymer particle
Protein adsorption suppression
Seeded dispersion polymerization
Metal organic frameworks

ABSTRACT

Golf ball-like polymer particles, characterized by their distinctive concave–convex surface morphology, have been used as catalyst supports and coating materials owing to their high specific surface area and shape-derived properties. However, site-selective surface functionalization and postsynthetic incorporation of additional functionalities have rarely been investigated. In this study, golf ball-like polymer particles bearing distinct functional groups on their convex and concave regions were fabricated via seeded dispersion polymerization in the presence of *n*-dodecane droplets. The resulting particles exhibited poly(ethylene glycol) groups on the convex regions, which suppressed nonspecific protein adsorption, while anionic carboxyl groups were localized on the concave regions, enabling electrostatic protein adsorption. Confocal laser scanning microscopy showed that fluorescence from FITC-conjugated proteins was selectively localized to the concave regions, confirming successful site-selective functionalization. Furthermore, metal–organic frameworks (MOFs) were synthesized on the concave surfaces via the carboxyl groups of the particles. These results demonstrate that golf ball-like polymer particles are promising candidates for highly sensitive and selective biosensing applications and serve as a versatile platform for constructing MOF–polymer hybrid materials, thereby considerably expanding the applicability of nonspherical polymer particles.

1. Introduction

In recent years, biosensing technologies have played a crucial role in diverse fields, including medical diagnostics, environmental monitoring, and food safety management, thereby driving the demand for highly sensitive and selective detection methods [1–7]. Polymeric particles have attracted considerable attention as promising materials for biosensing applications owing to their excellent chemical stability, ease of functionalization, and cost-effectiveness. Among the various factors influencing their performance, particle surface properties are known to strongly affect interactions with and adsorption of biomolecules [8–15]. Furthermore, optimization of surface morphology can facilitate the detection of fluorescence or other signal changes induced by target molecule adsorption, enabling highly sensitive sensing platforms [16].

In addition, metal–organic frameworks (MOFs) have been extensively investigated for a wide range of applications, including gas storage and separation, catalysis, and sensing [17–21]. In bio-related fields in particular, the intrinsic porosity of MOFs has been exploited for drug loading and controlled release [22,23]. However, in biological environments, nonspecific protein adsorption is known to degrade MOFs performance, prompting the development of effective strategies to suppress protein fouling on MOFs [24,25]. In this context, MOF–polymer hybrid materials have attracted increasing attention as a promising approach to inhibit protein adsorption while preserving the advantageous properties of MOFs [26].

Polymeric particles produced via heterogeneous polymerization techniques, such as dispersion or emulsion polymerization, typically adopt spherical morphologies owing to the minimization of interfacial free energy between the particles and the surrounding solvent. Therefore, the fabrication of nonspherical polymeric microparticles often requires alternative strategies, including the exploitation of particle–particle interactions, template-assisted synthesis, or post-polymerization physical deformation [27–30]. Among these approaches, seeded dispersion polymerization (SDP) in the presence of hydrocarbons has emerged as a particularly promising method because it enables the formation of nonspherical particles through in situ phase

* Corresponding author.
E-mail address: minamihi@kobe-u.ac.jp (H. Minami).

https://doi.org/10.1016/j.reactfunctpolym.2026.106861
Received 9 April 2026; Received in revised form 18 June 2026; Accepted 3 July 2026
Available online 3 July 2026
1381-5148/© 2026 The Authors. Published by Elsevier B.V. This is an open access article under the CC BY-NC license (http://creativecommons.org/licenses/by-nc/4.0/).

separation during polymerization [31–39]. In particular, golf ball-like polymer particles with concave–convex surface morphologies have attracted considerable attention because of their unique surface structures and potential applications in sensing and colloidal assembly [40–43,49,50].

In our previous work, polystyrene (PS) particles bearing sulfate groups were used as seeds for the SDP of *n*-butyl methacrylate (*n*BMA) in the presence of hydrocarbons, resulting in composite particles containing multiple domains composed of poly(*n*-butyl methacrylate) (P*n*BMA) and hydrocarbons [44]. Subsequent extraction of the hydrocarbons yielded nonspherical PS particles featuring dimpled structures coated with P*n*BMA. These particles exhibited partial surface functionalization, retaining negative charges derived from sulfate groups on the convex regions; however, the integration of multiple functionalities into spatially distinct surface area and post-synthetic introduction of additional functionalities remained unexplored.

Additionally, site-selective functionalization of polymeric materials has attracted considerable attention because spatially controlled surface chemistry enables selective immobilization of biomolecules and localized sensing functions. Shin et al. demonstrated pore-selective immobilization of functional polymers and enzymes in porous polymer films prepared by breath figure methods, where functional groups were selectively introduced into pore interiors to create microreactor-like environments for biosensing applications [45]. However, despite these advances in two-dimensional porous films, site-selective functionalization of nonspherical polymer particles possessing three-dimensional concave–convex surface structures remained unexplored.

In this study, we fabricated golf ball-like polymer microparticles with site-specific functionalization on both concave and convex regions. Specifically, seed particles bearing hydrophilic poly(ethylene glycol) (PEG) groups and the carboxyl-functional initiator 4,4′-azobis(4-cyanovaleric acid) (V-501) were used in SDP in the presence of *n*-dodecane. This strategy enabled the formation of particles featuring PEG groups on the convex regions and carboxyl groups on the concave regions. As a result, nonspecific protein adsorption was effectively suppressed on the convex regions, while proteins were preferentially adsorbed onto the concave regions. Furthermore, we demonstrate that the carboxyl groups localized in the concave regions act as anchoring sites for the selective formation of MOFs in the concavities.

2. Experimental section

2.1. Materials

Styrene was purchased from Nacalai Tesque, Inc. (Kyoto, Japan) and purified using an alumina column to remove inhibitor residues. *tert*-Butyl methacrylate (*t*BMA) was obtained from Tokyo Chemical Industry Co. (Tokyo, Japan) and purified using an alumina column. The initiator 2,2′-azobis(isobutyronitrile) (AIBN; FUJIFILM Wako Pure Chemical Co., Osaka, Japan) was purified by recrystallization from methanol. Poly (ethylene glycol) methacrylate (PEGMA: Mn = 360) and fluorescein isothiocyanate–conjugated avidin from egg white (avidin–FITC) were purchased from Sigma-Aldrich Japan (Tokyo, Japan) and used as received. Poly(vinylpyrrolidone) (PVP, K-30: Mw = 4.0×10^4), sodium chloride (NaCl), and zinc nitrate hexahydrate ($Zn(NO_3)_2{\cdot}6H_2O$) were obtained from Nacalai Tesque, Inc. (Kyoto, Japan) and used without further purification. Furthermore, V-501, sodium dihydrogen phosphate, and disodium hydrogen phosphate were purchased from FUJIFILM Wako Pure Chemical Co. (Osaka, Japan) and used as received. Methanol, ethanol, *n*-dodecane, and 2-methylimidazole (2-MIM) were obtained from Tokyo Chemical Industry Co. (Tokyo, Japan) and used without further purification. Ruthenium tetraoxide (RuO_4) was purchased from Filgen, Inc. (Aichi, Japan) and used as received. Deionized water was purified using an ElixUV system (Merck Millipore, Tokyo, Japan) to a resistivity greater than 5 MΩ·cm.

2.2. Preparation of the poly(vinylpyrrolidone)-stabilized polystyrene (PS_{PVP}) particles by dispersion polymerization

Styrene (200 g), PVP (K-30, 30 g), and AIBN (2 g) were dissolved in ethanol (600 g) and transferred to a separate flask (2000 mL). The mixture was stirred at 120 rpm in a water bath at 60 °C for 24 h under an N_2 atmosphere. The resulting PVP-stabilized PS particles (PS_{PVP}) were collected and washed with methanol by centrifugation at 3000 ×*g* for 5 min.

2.3. Preparation of the PS_{PVP}/P(S-co-PEGMA) particles by seeded-dispersion polymerization

Styrene (1.0 g), PEGMA (1.0 g), and AIBN (0.040 g) were dissolved in a mixture of methanol (16.0 g) and water (4.0 g). The resulting solution was transferred to a glass tube, into which PS_{PVP} seed particles (2.0 g) were dispersed. The glass tube was then sealed under an N_2 atmosphere and horizontally shaken in a water bath at 60 °C for 24 h at 70 cycles min^{-1} with a stroke length of 3 cm. After polymerization, the resulting PS core–shell particles bearing PEG-derived hydrophilic groups (PS_{PVP}/poly(styrene-*co*-PEGMA) (P(S-*co*-PEGMA))) were collected and washed with methanol by centrifugation at 2040 rpm (500 ×*g*) for 5 min.

2.4. Preparation of golf ball-like PS_{PVP}/P(S-co-PEGMA)/PtBMA particles by seeded dispersion polymerization

A typical SDP procedure was performed as follows. *t*BMA (0.15 g) and V-501 (1.5 mg) were dissolved in a mixture of methanol (4.0 g) and water (1.0 g) and transferred to a glass tube. The PS_{PVP}/P(S-*co*-PEGMA) seed particles (0.25 g) and *n*-dodecane (0.25 g) were then dispersed in the solution. The glass tube was sealed under an N_2 atmosphere and horizontally shaken in a water bath at 60 °C for 24 h at 70 cycles min^{-1} with a stroke length of 3 cm. After polymerization, the resulting golf ball-like PS_{PVP}/P(S-*co*-PEGMA)/poly(*t*BMA) (P*t*BMA) particles were washed with methanol by centrifugation at 2040 rpm (500 ×*g*) for 5 min to remove *n*-dodecane. The dispersion medium was subsequently exchanged to water by centrifugation at 6450 rpm (5000 ×*g*) for 5 min.

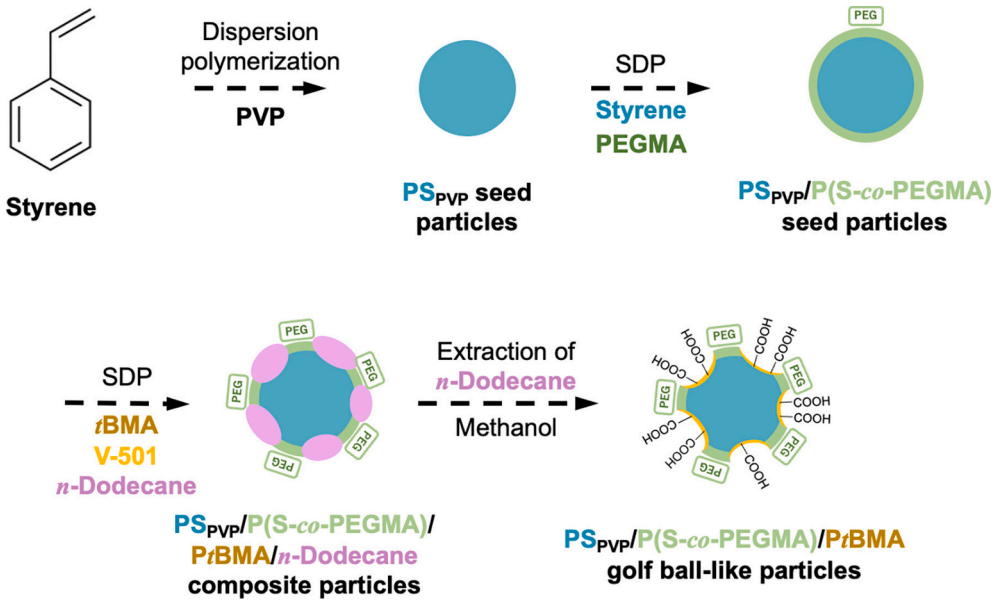
To control the morphology of the particle surface, we varied the polymerization temperature and the amount of the second monomer, respectively. The polymerization temperature was varied between 40 °C and 70 °C. The seed particles/*t*BMA ratios were varied between 1/0.6 and 1/0.2 (*w*/w).

2.5. Adsorption of avidin-FITC onto PS_{PVP}, PS_{PVP}/P(S-co-PEGMA), or PS_{PVP}/P(S-co-PEGMA)/PtBMA particles

The prepared particles were measured so that their total surface area reached 5.2×10^{13} nm^2 and were then vacuum-dried [46]. Subsequently, the particles were dispersed in 90 μL of 10 mM phosphate-buffered saline (PBS; 140 mM NaCl, pH 7). To this suspension, 10 μL of an avidin–FITC solution (0.6 nmol mL^{-1} in PBS) was added, and the mixture was incubated in the dark for 24 h. Finally, the samples were analyzed by confocal laser scanning microscopy (CLSM; STELLARIS 8, Leica, Germany).

2.6. Synthesis of metal-organic frameworks on PS_{PVP}/P(S-co-PEGMA)/PtBMA particles

2-MIM (16.6 mg) was dissolved in a mixture of methanol (800 μL) and water (100 μL) and transferred to a 1.5 mL microtube. The PS_{PVP}/P(S-*co*-PEGMA)/P*t*BMA particles (1.0 mg) were dispersed in this solution. Thereafter, $Zn(NO_3)_2{\cdot}6H_2O$ (1.5 mg) was dissolved in methanol (100 μL) and added dropwise to the dispersion for 1 min while stirring, and the mixture was gently stirred at 25 °C for 1 min. After completion of the reaction, the resulting MOFs@PS_{PVP}/P(S-*co*-PEGMA)/P*t*BMA particles were collected and washed with methanol by filtration.



Scheme 1. Preparation of golf ball-like polymer microparticles with site-specific functionalization on both concave and convex regions via SDP.

2.7. Characterization

The obtained particles were analyzed using a scanning electron microscope (SEM; JSM-IT700HR, JEOL, Tokyo, Japan) operated at an accelerating voltage of 5 kV and further characterized by an SEM instrument equipped with energy-dispersive X-ray spectroscopy (EDS; JEOL EX-74212U4L2Q). The number-average diameter (D_n) and coefficient of variation (C_V) were determined by analyzing more than 200 particles using image analysis software (ImageJ 1.54 g; Wayne Rasband and contributors, National Institutes of Health, USA). To investigate the components of the PS_{PVP}/P(S-*co*-PEGMA)/P*t*BMA particles, thermogravimetric analysis (TGA) was conducted using a TGA instrument (TG/DTA 7200, Hitachi High-Tech, Tokyo, Japan). Dried samples were heated up to 600 °C under nitrogen atmospheres at a heating rate of 10 °C min^{-1}. To investigate the internal morphology of the PS_{PVP}/P(S-*co*-PEGMA)/P*t*BMA particles and MOFs@PS_{PVP}/P(S-*co*-PEGMA)/P*t*BMA particles, ultrathin sections (approximately 100 nm thick) were prepared from dried particles embedded in an epoxy resin using an ultramicrotome (Leica EM UC6 equipped with EM FC7, Tokyo, Japan). In addition, the PS_{PVP}/P(S-*co*-PEGMA)/P*t*BMA particles were stained with RuO_4 vapor at room temperature for 30 min in the presence of RuO_4 crystals and then kept overnight at room temperature. The resulting ultrathin cross sections were subsequently observed by transmission electron microscopy (TEM; JEOL JEM-1230, Tokyo, Japan) instrument operated at an accelerating voltage of 100 kV. To further investigate the internal morphology of the PS_{PVP}/P(S-*co*-PEGMA)/P*t*BMA particles, cross-section samples were prepared by a cross-section polisher (CP; IB-19530CP, JEOL, Tokyo, Japan) and observed by SEM. To characterize the chemical properties of the PS_{PVP}/P(S-*co*-PEGMA)/P*t*BMA particles, an Fourier transform infrared spectrometer (FT-IR; FT/IR-6000, JASCO, Tokyo, Japan) measurement was performed. To investigate the formation of MOF crystals on the golf ball-like particles, small-angle incidence X-ray diffraction (XRD) measurements were performed with a SmartLab (Rigaku Co.) at 30 mA and 40 kV. The scanning speed was 2 s/step for out of plane., step size was 0.1° and the scanning range of 2θ was from 3° to 80°. The footprint of the X-ray beam was set at 15 mm × 15 mm. The CuKα X-ray beam ($\lambda = 1.5418$ Å) was irradiated with the incient angle of 0.06°.

3. Results and discussion

The preparation of golf ball-like polymer microparticles with site-specific functionalization on both concave and convex regions was carried out as shown in Scheme 1. Micron-sized, monodisperse PS particles bearing PEG-functionalized surfaces were prepared via SDP. Initially, spherical PS_{PVP} particles were synthesized by dispersion

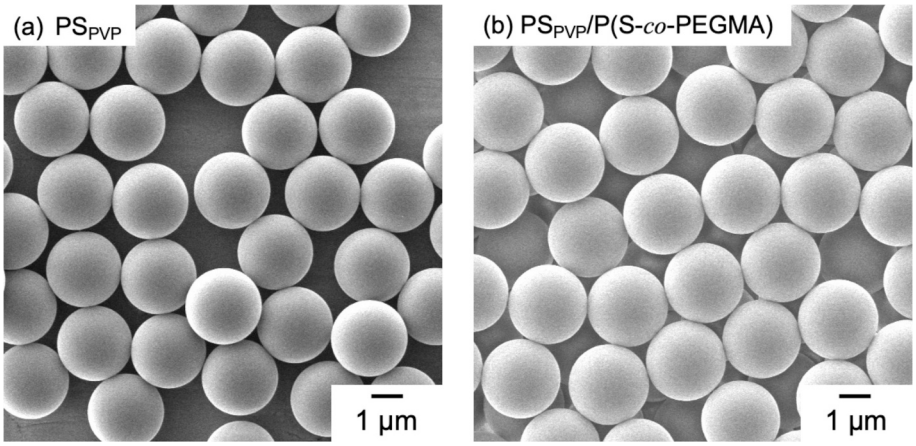


Fig. 1. SEM images of PS_{PVP} particles prepared by dispersion polymerization (a) and PS_{PVP}/P(S-*co*-PEGMA) particles prepared by SDP (b).

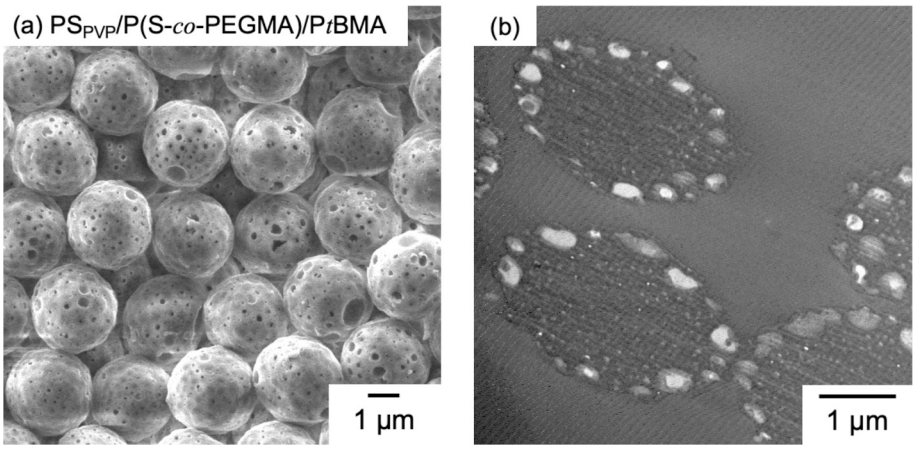


Fig. 2. SEM image of PS$_{PVP}$/P(S-*co*-PEGMA)/P*t*BMA golf ball-like particles after *n*-dodecane extraction with methanol (a) and TEM image of an ultrathin cross-section of a golf ball-like particle after RuO_4 staining (b).

polymerization of styrene using PVP as a dispersion stabilizer (Fig. 1a). Subsequently, styrene and PEGMA were subjected to SDP using the PS$_{PVP}$ particles as seeds, yielding PS particles with PEG-modified surfaces that suppressed protein adsorption (PS$_{PVP}$/P(S-*co*-PEGMA), Fig. 1b). Additionally, the resulting particles exhibited excellent colloidal stability from room temperature up to 60 °C despite the absence of an added dispersion stabilizer. This stability is attributed to the PEGMA component, which likely acted as an effective steric stabilizer. Both PS$_{PVP}$ and PS$_{PVP}$/P(S-*co*-PEGMA) particles were spherical and highly monodisperse, with D_n and C_V of 2.34 μm and 1.9%, respectively, for PS$_{PVP}$, and 2.44 μm and 1.2%, respectively, for PS$_{PVP}$/P(S-*co*-PEGMA). The observed increase in particle size while maintaining monodispersity confirms the successful execution of the SDP process.

To prepare the golf ball-like particles, SDP of *t*BMA was performed in a methanol/water medium (80/20, *w*/w) in the presence of *n*-dodecane droplets using PS$_{PVP}$/P(S-*co*-PEGMA) particles as seeds. After polymerization, the particles were washed with methanol to remove *n*-dodecane because methanol is a poor solvent for both P*t*BMA and PS. Fig. 2a shows an SEM image of the resulting PS$_{PVP}$/P(S-*co*-PEGMA)/P*t*BMA particles, clearly demonstrating the formation of golf ball-like morphologies. In addition, PS$_{PVP}$/P(S-*co*-PEGMA)/P*t*BMA particles were also spherical and monodisperse, with D_n and C_V of 2.75 μm and 3.6%, respectively. To further examine the internal structure, ultrathin cross sections of the particles were prepared using a microtome, stained with RuO_4, and observed by TEM (Fig. 2b), where the PS phase was selectively stained and appeared as dark regions, while the P*t*BMA phase was observed as bright regions. The concave surfaces of the particles were covered with the P*t*BMA phase, which appeared as bright regions in the images, whereas the PS phase covered the convex surfaces. Moreover, to characterize the chemical properties, FT-IR measurement of the particles was performed (Fig. S1). The FT-IR spectra showed characteristic absorption bands attributed to ester groups derived from P*t*BMA and P(S-*co*-PEGMA) and aromatic groups derived from PS, supporting the successful formation of the composite polymer particles. In addition, to investigate the components of the golf ball-like particles, TGA was conducted (Fig. S2). TGA profile supported the presence of PS and PEG in the particles. This morphology can be rationalized by a precipitation- and domain-formation process during SDP. As the polymerization progressed, the second polymer, P*t*BMA, became insoluble under the reaction conditions and precipitated onto the PS$_{PVP}$/P(S-*co*-PEGMA) seed

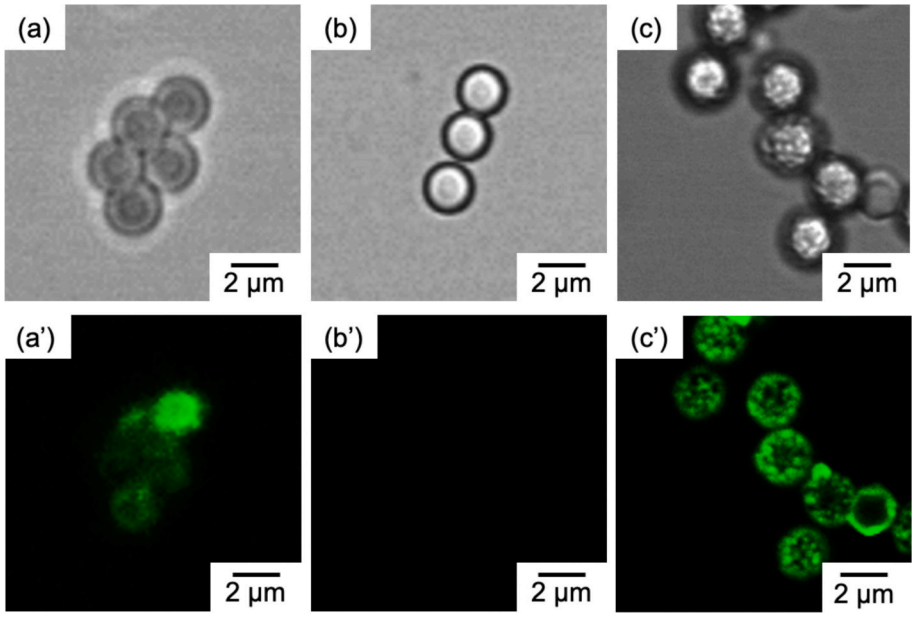


Fig. 3. CLSM images of PS$_{PVP}$ particles (a, a'), PS$_{PVP}$/P(S-*co*-PEGMA) particles (b, b'), and PS$_{PVP}$/P(S-*co*-PEGMA)/P*t*BMA particles (c, c') coincubated with avidin–FITC for 24 h at 25 °C. The samples were excited at 488 nm.

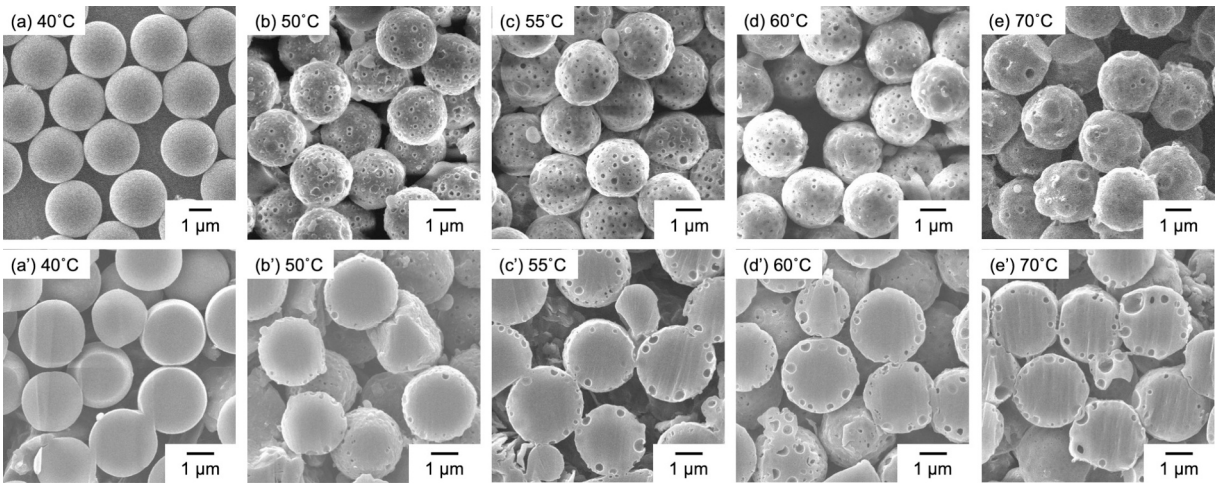


Fig. 4. SEM images of surfaces (a-e) and cross sections (a'-e') of the PS_{PVP}/P(S-*co*-PEGMA)/P*t*BMA particles after extracting *n*-dodecane from the composite particles prepared by *t*BMA SDP in the presence of *n*-dodecane droplets at various temperatures.

particles, forming P*t*BMA-rich domains on the seed surface. Importantly, because the hydrocarbon exhibited a higher affinity for the second polymer than for the seed polymer, it was preferentially absorbed into the P*t*BMA-rich domains. Therefore, once P*t*BMA domains with a high affinity for *n*-dodecane formed, *n*-dodecane migrated from the surrounding medium into these P*t*BMA-rich regions. This selective uptake of *n*-dodecane caused swelling of the P*t*BMA domains, resulting in the formation of P*t*BMA/*n*-dodecane composite domains. When the viscosity of the seed particles was sufficiently high, coalescence of these domains was strongly suppressed, preserving their discrete distribution on the surface of the composite particles. Finally, after completion of the polymerization, removal of the hydrocarbon (*n*-dodecane) produced concave structures corresponding to the former domain regions on the particle surface, in which the second polymer (P*t*BMA) remained[34–38].

To confirm that the ability to suppress nonspecific protein adsorption was present only on the convex regions of the particles, an avidin–FITC solution in PBS (pH 7) was added to dispersions of the seed particles (PS_{PVP} and PS_{PVP}/P(S-*co*-PEGMA)) and the golf ball-like particles (PS_{PVP}/P(S-*co*-PEGMA)/P*t*BMA) in PBS (pH 7), and the samples were observed by CLSM. Because the isoelectric point of avidin is approximately pH 10, avidin is expected to be positively charged under these conditions and therefore to interact strongly with negatively charged carboxyl groups via electrostatic interactions. In addition, avidin is also considered to adsorb onto P*t*BMA in the concave regions via hydrophobic interactions. Fig. 3 shows CLSM images of the seed particles and the golf ball-like particles before and after exposure to avidin–FITC, and, as shown in Figs. 3a–3a', clear adsorption of avidin was observed for particles whose surfaces were composed of PVP and PS. In contrast, PS_{PVP}/P(S-*co*-PEGMA) particles exhibited no detectable avidin adsorption, as shown in Figs. 3b–3b'. For the PS_{PVP}/P(S-*co*-PEGMA)/P*t*BMA particles, avidin-derived fluorescence appeared as discrete, patchy spots, and comparison of the corresponding bright-field and fluorescence images revealed that the fluorescence was localized only in the concave regions (Figs. 3c–3c'). These observations clearly demonstrate that the suppression of nonspecific protein adsorption is confined to the convex regions of the particles. These results suggest that both electrostatic and hydrophobic interactions contribute to protein adsorption in the concave regions.

To further investigate the effect of polymerization temperature on particle morphology, cross-sectional observations were performed for particles prepared at different temperatures using CP. From Fig. 4, no concave regions were observed for the particles prepared at 40 °C, whereas small and shallow concave regions were observed at 50 °C. Increasing the polymerization temperature to 55 and 60 °C resulted in the formation of larger and deeper concave regions. At 70 °C, the concave regions became wider, although their depth did not significantly increase. These results indicate that a higher polymerization temperature led to the formation of concavities with a larger aperture due to the coalescence of the domains that formed on the seed particles. This morphological change was likely due to the lower viscosity of the seed particles at higher temperatures, which promotes the submersion of the P*t*BMA domains into the seeds. In addition, the absence of concave structures at 40 °C was likely due to insufficient polymerization activity of V-501 at this temperature, resulting in insufficient formation of the second polymer phase. Furthermore, decreasing the amount of the second monomer (*t*BMA) resulted in smoother particle surfaces with smaller concave structures, suggesting that monomer concentration also influences the morphology of the obtained particles (Fig. S3). These results are consistent with our previous report[39].

Subsequently, to further exploit the functionalized concave regions, we attempted to grow MOFs on the carboxyl-functionalized concaves of the golf ball-like particles. The MOFs were synthesized using Zn^{2+} as the metal source and 2-MIM as the organic ligand because MOFs derived from Zn^{2+} and 2-MIM have previously been reported to form on

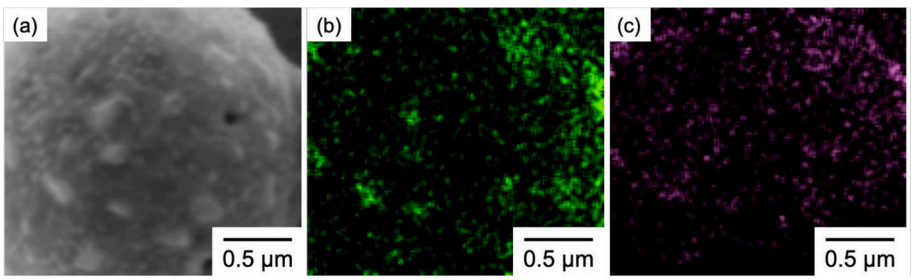


Fig. 5. SEM image of the MOFs@PS_{PVP}/P(S-*co*-PEGMA)/P*t*BMA particle (a) and EDS elemental maps of Zn (b) and N (c) for the corresponding particle.

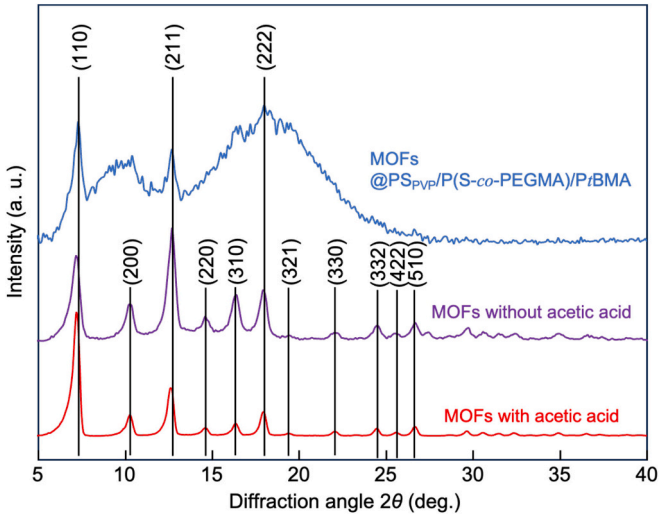


Fig. 6. X-ray diffraction profiles of the MOFs@PS$_{PVP}$/P(S-*co*-PEGMA)/P*t*BMA, MOFs without acetic acid, and MOFs with acetic acid.

carboxyl-functionalized surfaces [47]. Fig. 5 shows SEM images and the corresponding EDS elemental maps of the resulting MOFs@PS$_{PVP}$/P(S-*co*-PEGMA)/P*t*BMA particles. Compared with the particles prior to MOFs synthesis, the concave regions were filled with newly formed material, and protrusion-like structures were clearly observed. EDS mapping revealed pronounced localization of Zn and N in these protrusions, indicating that they originated from the formation of MOFs composed of Zn^{2+} and 2-MIM. In addition, ultrathin cross sections of the particles after MOFs growth were prepared using a microtome and examined by TEM (Fig. S4), which revealed dark, electron-dense features surrounding the P*t*BMA phase in the concave regions. Although a small amount of MOF formation was also observed on the convex surfaces, MOF growth preferentially proceeded in the concave regions under the present reaction conditions. In addition, when the reaction time was prolonged, MOF formation gradually proceeded over the entire particle surface (Fig. S5). Furthermore, XRD measurements were performed to confirm the formation of MOF crystals on the golf ball-like particles (Fig. 6). The diffraction peaks assignable to ZIF-8 were clearly observed for the MOFs and the MOF–golf ball-like particle composites [48]. These results support the successful formation of ZIF-8 on the particle surfaces. These observations and measurements confirm that MOF formation occurred selectively at the carboxyl-group-bearing concaves of the particles.

4. Conclusions

We successfully fabricated golf ball-like polymer particles bearing distinct functionalities on both convex and concave regions by subjecting *t*BMA to SDP in the presence of *n*-dodecane droplets. The resulting particles exhibited suppression of nonspecific protein adsorption on the convex regions, while anionic functional groups and hydrophobic polymer localized on the concave regions enabled selective biomolecular adsorption. Moreover, the morphology of the golf ball-like polymer particles could be tuned by varying the reaction temperature and the amount of second monomer during polymerization. We further demonstrated selective growth of MOFs in the concave regions, highlighting the utility of these particles as polymer-MOF hybrid platforms. Although the present system predominantly yielded golf ball-like morphology because of the highly hydrophilic nature of the PEG-bearing seed particles, the results demonstrated the possibility of introducing multiple functionalities into nonspherical polymer particles. These findings provide a useful strategy for site-selective functionalization of nonspherical polymer particles and expand their potential applications in biosensing and biointerface materials.

CRediT authorship contribution statement

Takahiro Morishita: Writing – original draft, Methodology, Investigation, Data curation. **Rintaro Furukawa:** Data curation, Investigation. **Takuya Matsumoto:** Data curation, Supervision. **Nozomu Suzuki:** Writing – review & editing, Validation, Supervision, Methodology. **Toyoko Suzuki:** Writing – review & editing, Supervision, Conceptualization. **Hideto Minami:** Writing – review & editing, Supervision, Project administration, Methodology, Funding acquisition, Data curation, Conceptualization.

Declaration of competing interest

The authors declare that they have no known competing financial interests or personal relationships that could have appeared to influence the work reported in this paper.

Acknowledgment

This work was partially supported by Grant-in-Aid for Scientific Research (Grant No. 23H02025) from the Japan Society for the Promotion of Science (JSPS).

Appendix A. Supplementary data

Supplementary data to this article can be found online at https://doi.org/10.1016/j.reactfunctpolym.2026.106861.

Data availability

Data will be made available on request.

References

[1] E. Guler, H.C. Soyleyici, D.O. Demirkol, M. Ak, S. Timur, A novel functional conducting polymer as an immobilization platform, Mater. Sci. Eng. C 40 (2014) 148–156, https://doi.org/10.1016/j.msec.2014.03.063.
[2] H. Akbulut, G. Bozokalfa, D.N. Asker, B. Demir, E. Guler, D.O. Demirkol, S. Tirnur, Y. Yagci, Polythiophene-*g*-poly(ethylene glycol) with lateral amino groups as a novel matrix for biosensor construction, ACS Appl. Mater. Interfaces 7 (37) (2015) 20612–20622, https://doi.org/10.1021/acsami.5b04967.
[3] T. Yilmaz, E. Guler, Z.P. Gumus, H. Akbulut, E. Aldemir, H. Coskunol, D.G. Colak, I. Cianga, S. Yamada, S. Timur, T. Endo, Y. Yagci, Synthesis and application of a novel poly-L-phenylalanine electroactive macromonomer as matrix for the biosensing of 'abused drug' model, Polym. Chem. 7 (47) (2016) 7304–7315, https://doi.org/10.1039/c6py01764a.
[4] T.Y. Sengel, E. Guler, Z.P. Gumus, E. Aldemir, H. Coskunol, H. Akbulut, D.G. Colak, I. Cianga, S. Yamada, S. Timur, T. Endo, Y. Yagci, An Immunoelectrochemical platform for the biosensing of 'cocaine use', Sens. Actuators B 246 (2017) 310–318, https://doi.org/10.1016/j.snb.2017.02.087.
[5] K.M. Lee, K.H. Kim, H. Yoon, H. Kim, Chemical Design of Functional Polymer Structures for biosensors: from nanoscale to macroscale, Polymers 10 (5) (2018) 551, https://doi.org/10.3390/polym10050551.
[6] L.Z. Xu, R. Chopdat, D.Y. Li, K.T. Al-Jamal, Development of a simple, sensitive and selective colorimetric aptasensor for the detection of cancer-derived exosomes, Biosens. Bioelectron. 169 (2020) 112576, https://doi.org/10.1016/j.bios.2020.112576.
[7] F. Bialas, D. Reichinger, C.F.W. Becker, Biomimetic and biopolymer-based enzyme encapsulation, Enzym. Microb. Technol. 150 (2021) 109864, https://doi.org/10.1016/j.enzmictec.2021.109864.
[8] J.H. Park, Y.H. Bae, Hydrogels based on poly(ethylene oxide) and poly (tetramethylene oxide) or poly(dimethyl siloxane): synthesis, characterization, in vitro protein adsorption and platelet adhesion, Biomaterials 23 (8) (2002) 1797–1808, https://doi.org/10.1016/S0142-9612(01)00306-4.
[9] P. Kingshott, J. Wei, D. Bagge-Ravn, N. Gadegaard, L. Gram, Covalent attachment of poly(ethylene glycol) to surfaces, critical for reducing bacterial adhesion, Langmuir 19 (17) (2003) 6912–6921, https://doi.org/10.1021/la034032m.
[10] J.W. Zhou, A.V. Ellis, N.H. Voelcker, Recent developments in PDMS surface modification for microfluidic devices, Electrophoresis 31 (1) (2010) 2–16, https://doi.org/10.1002/elps.200900475.
[11] S. Yoshida, K. Hagiwara, T. Hasebe, A. Hotta, Surface modification of polymers by plasma treatments for the enhancement of biocompatibility and controlled drug

release, Surf. Coat. Technol. 233 (2013) 99–107, https://doi.org/10.1016/j.surfcoat.2013.02.042.
[12] C. Yang, X. Ding, R.J. Ono, H. Lee, L.Y. Hsu, Y.W. Tong, J. Hedrick, Y.Y. Yang, Brush-like polycarbonates containing dopamine, cations, and PEG providing a broad-spectrum, antibacterial, and antifouling surface via one-step coating, Adv. Mater. 26 (43) (2014) 7346–7351, https://doi.org/10.1002/adma.201402059.
[13] A. Miodek, E.M. Regan, N. Bhalla, N.A.E. Hopkins, S.A. Goodchild, P. Estrela, Optimisation and characterisation of anti-fouling ternary SAM layers for impedance-based aptasensors, Sensors 15 (10) (2015) 25015–25032, https://doi.org/10.3390/s151025015.
[14] A. Khlyustova, Y.F. Cheng, R. Yang, Vapor-deposited functional polymer thin films in biological applications, J. Mater. Chem. B 8 (31) (2020) 6588–6609, https://doi.org/10.1039/d0tb00681e.
[15] X.H. Zhou, B. Zheng, Surface modification for improving immunoassay sensitivity, Lab Chip 23 (5) (2023) 1151–1168, https://doi.org/10.1039/d2lc00811d.
[16] K. Mori, M. Hirase, T. Morishige, E. Takano, H. Sunayama, Y. Kitayama, S. Inubushi, R. Sasaki, M. Yashiro, T. Takeuchi, A pretreatment-free, polymer-based platform prepared by molecular imprinting and post-imprinting modifications for sensing intact exosomes, Angew. Chem. Int. Ed. 58 (6) (2019) 1612–1615, https://doi.org/10.1002/anie.201811142.
[17] C.L. Hobday, C.H. Woodall, M.J. Lennox, M. Frost, K. Kamenev, T. Düren, C. A. Morrison, S.A. Moggach, Understanding the adsorption process in ZIF-8 using high pressure crystallography and computational modelling, Nat. Commun. 9 (1) (2018) 1429, https://doi.org/10.1038/s41467-018-03878-6.
[18] B.C. Ma, T. Yao, X.Z. Meng, Y. Xu, Z.F. Ma, H.L. Han, Novel immunoprobe based on MOF-818 synergizing with an antifouling sensing interface to improve immunosensors, ACS Sustain. Chem. Eng. 10 (36) (2022) 12041–12047, https://doi.org/10.1021/acssuschemeng.2c04356.
[19] Y. Liang, X.X. Yang, X.Y. Wang, Z.J. Guan, H. Xing, Y. Fang, A cage-on-MOF strategy to coordinatively functionalize mesoporous MOFs for manipulating selectivity in adsorption and catalysis, Nat. Commun. 14 (1) (2023) 5223, https://doi.org/10.1038/s41467-023-40973-9.
[20] M. Saghian, S. Dehghanpour, Z. Bayatani, A. Facile, Rapid procedure for Knoevenagel condensation reaction catalyzed by efficient amino-bifunctional frameworks under mild conditions, Sci. Rep. 13 (1) (2023) 15563, https://doi.org/10.1038/s41598-023-42832-5.
[21] Y.Q. Jiao, Z.S. Du, Q.Y. Xie, X.N. Wen, W.S. Zhang, J.W. Zhu, G.W. Lu, G.G. Zhou, Z.Q. Yang, Y.H. Xia, Study on gas adsorption and separation performance of alkyl functionalized MOF materials under wet conditions, RSC Adv. 15 (4) (2025) 2608–2617, https://doi.org/10.1039/d4ra08720h.
[22] I.A. Lázaro, S. Haddad, S. Sacca, C. Orellana-Tavra, D. Fairen-Jimenez, R.S. Forgan, Selective surface PEGylation of UiO-66 nanoparticles for enhanced stability, cell uptake, and pH-responsive drug delivery, Chem 2 (4) (2017) 561–578, https://doi.org/10.1016/j.chempr.2017.02.005.
[23] V.A. Tran, S.W. Lee, pH-triggered degradation and release of doxorubicin from Zeolitic Imidazolate Framework-8 (ZIF8) decorated with polyacrylic acid, RSC Adv. 11 (16) (2021) 9222–9234, https://doi.org/10.1039/d0ra10423j.
[24] N. Gan, Q.M. Sun, L.D. Zhao, P.X. Tang, Z.L. Suo, S.S. Zhang, Y.K. Zhang, M. Zhang, W.J. Wang, H. Li, Protein corona of metal-organic framework nanoparticals: study on the adsorption behavior of protein and cell interaction, Int. J. Biol. Macromol. 140 (2019) 709–718, https://doi.org/10.1016/j.ijbiomac.2019.08.183.
[25] A. Mittal, S. Gandhi, I. Roy, Mechanistic interaction studies of synthesized ZIF-8 nanoparticles with bovine serum albumin using spectroscopic and molecular docking approaches, Sci. Rep. 12 (1) (2022) 10331, https://doi.org/10.1038/s41598-022-14630-y.
[26] M.S. Ural, J.M. Joseph, F. Wien, X. Li, M.A. Tran, M. Taverna, C. Smadja, R. Gref, A comprehensive investigation of the interactions of human serum albumin with polymeric and hybrid nanoparticles, Drug Delivery Transl. Res. 14 (8) (2024) 2188–2202, https://doi.org/10.1007/s13346-024-01578-x.
[27] K.C. Ho, W.M. Yeh, T.S. Tung, J.Y. Liao, Amperometric detection of morphine based on poly(3,4-ethylenedioxythiophene) immobilized molecularly imprinted polymer particles prepared by precipitation polymerization, Anal. Chim. Acta 542 (1) (2005) 90–96, https://doi.org/10.1016/j.aca.2005.02.036.
[28] J.A. Champion, Y.K. Katare, S. Mitragotri, Making polymeric micro- and nanoparticles of complex shapes, Proc. Natl. Acad. Sci. 104 (29) (2007) 11901–11904, https://doi.org/10.1073/pnas.0705326104.
[29] H. Minami, Y. Mizuta, T. Suzuki, Preparation of raspberry-like polymer particles by a heterocoagulation technique utilizing hydrogen bonding interactions between steric stabilizers, Langmuir 29 (2) (2013) 554–560, https://doi.org/10.1021/la3043507.
[30] S. Raza, X.Y. Yong, B.W. Yang, R.W. Xu, J.P. Deng, Biomass trans-Anethole-based hollow polymer particles: preparation and application as sustainable absorbent, ACS Sustain. Chem. Eng. 5 (11) (2017) 10011–10018, https://doi.org/10.1021/acssuschemeng.7b01956.
[31] M. Okubo, Y. Murakami, T. Fujiwara, Formation mechanism of anomalous “golf ball-like” composite polymer particles by seeded emulsion polymerization, Colloid Polym. Sci. 274 (6) (1996) 520–524, https://doi.org/10.1007/Bf00655226.
[32] M. Okubo, T. Fujiwara, A. Yamaguchi, Morphology of anomalous polystyrene/polybutyl acrylate composite particles produced by seeded emulsion polymerization, Colloid Polym. Sci. 276 (2) (1998) 186–189, https://doi.org/10.1007/s003960050227.
[33] M. Okubo, A. Yamaguchi, T. Fujiwara, Thermodynamic aspects of the heterogeneous structure of “golf-ball-like” polymer particles, Colloid Polym. Sci. 277 (10) (1999) 1005–1008, https://doi.org/10.1007/s003960050483.
[34] M. Okubo, R. Takekoh, A. Suzuki, Preparation of Micron-sized, monodisperse poly (methyl methacrylate)/polystyrene composite particles having a large number of dents on their surfaces by seeded dispersion polymerization in the presence of Decalin, Colloid Polym. Sci. 280 (11) (2002) 1057–1061, https://doi.org/10.1007/s00396-002-0661-8.
[35] T. Fujibayashi, M. Okubo, Preparation and thermodynamic stability of micron-sized, monodisperse composite polymer particles of disc-like shapes by seeded dispersion polymerization, Langmuir 23 (15) (2007) 7958–7962, https://doi.org/10.1021/la7007842.
[36] T. Fujibayashi, Y. Komatsu, N. Konishi, H. Yamori, M. Okubo, Effect of polymer polarity on the shape of “golf ball-like” particles prepared by seeded dispersion polymerization, Ind. Eng. Chem. Res. 47 (17) (2008) 6445–6449, https://doi.org/10.1021/ie800188f.
[37] N. Konishi, T. Fujibayashi, T. Tanaka, H. Minami, M. Okubo, Effects of properties of the surface layer of seed particles on the formation of golf ball-like polymer particles by seeded dispersion polymerization, Polym. J. 42 (1) (2010) 66–71, https://doi.org/10.1038/pj.2009.313.
[38] T. Fujibayashi, T. Tanaka, H. Minami, M. Okubo, Thermodynamic and kinetic considerations on the morphological stability of “hamburger-like” composite polymer particles prepared by seeded dispersion polymerization, Colloid Polym. Sci. 288 (8) (2010) 879–886, https://doi.org/10.1007/s00396-010-2211-0.
[39] T. Morishita, H. Ikeda, N. Suzuki, T. Suzuki, H. Minami, Morphology control of poly(methyl methacrylate) particles via seeded dispersion polymerization, Next Mater. 10 (2026) 101432, https://doi.org/10.1016/j.nxmate.2025.101432.
[40] M. Dai, L. Song, W. Nie, Y. Zhou, Golf ball-like particles fabricated by nonsolvent/solvent-induced phase separation method, J. Colloid Interface Sci. 391 (2013) 168–171, https://doi.org/10.1016/j.jcis.2012.07.097.
[41] J.H. Lee, C.-S. Lee, K.Y. Cho, Enhanced cell adhesion to the dimpled surfaces of golf-ball-shaped microparticles, ACS Appl. Mater. Interfaces 6 (19) (2014) 16493–16497, https://doi.org/10.1021/am505997s.
[42] G.M.M. Sadeghi, A. Namjoo, S. Hosseinzadeh, S. Abdolbaghi, Y. Saadat, Facile method to synthesis of golf ball-like particles via early-ceased seeded dispersion polymerization, Polym. Sci. Ser. B 60 (5) (2018) 589–597, https://doi.org/10.1134/s1560090418050135.
[43] K. Watanabe, Y. Tajima, T. Shimura, H. Ishii, D. Nagao, Depletion-interaction-driven assembly of golf ball-like particles for development of colloidal macromolecules, J. Colloid Interface Sci. 534 (2019) 81–87, https://doi.org/10.1016/j.jcis.2018.08.117.
[44] T. Morishita, I. Maitani, T. Michiura, N. Suzuki, T. Suzuki, K. Akamatsu, H. Minami, Preparation of golf ball-like polymer particles bearing site-selective functional groups, ACS Appl. Mater. Interfaces 16 (46) (2024) 64058–64064, https://doi.org/10.1021/acsami.4c15686.
[45] B.K. Shin, P. Kulshrestha, A. Gandamalla, D. Huh, Pore-selective immobilization of pH-sensitive polymer and glucose oxidase in the porous polyimide film for detection of glucose, React. Funct. Polym. 204 (2024) 106027, https://doi.org/10.1016/j.reactfunctpolym.2024.106027.
[46] Y.R. Perera, J.X. Xu, D.L. Amarasekara, A.C. Hughes, I. Abbood, N.C. Fitzkee, Understanding the adsorption of peptides and proteins onto PEGylated gold nanoparticles, Molecules 26 (19) (2021) 5788, https://doi.org/10.3390/molecules26195788.
[47] H.J. Lee, W. Cho, M. Oh, Advanced fabrication of metal-organic frameworks: template-directed formation of polystyrene@ZIF-8 core-shell and hollow ZIF-8 microspheres, Chem. Commun. 48 (2) (2012) 221–223, https://doi.org/10.1039/c1cc16213f.
[48] A.M. Aboraia, A.A.A. Darwish, V. Polyakov, E. Erofeeva, V. Butova, H.Y. Zahran, A. F.A. El-Rehim, H. Algarni, I.S. Yahia, A.V. Soldatov, Structural characterization and optical properties of zeolitic imidazolate frameworks (ZIF-8) for solid-state electronics applications, Opt. Mater. 100 (2020) 109648, https://doi.org/10.1016/j.optmat.2019.109648.
[49] Y.F. Jiang, L. Zhao, R.S. Li, H. Zou, Golf ball-like polymer particles by colloidal etching, Langmuir 40 (49) (2024) 25811–25821, https://doi.org/10.1021/acs.langmuir.4c02773.
[50] N. Hano, Y. Takeda, S. Kanawa, N. Ryu, S. Nagaoka, R. Oda, H. Ihara, M. Takafuji, Fabrication of depth-controlled dimples on polymer microsphere and capturing of nano-sized objects, Coll. Surf. A. 697 (2024) 134321, https://doi.org/10.1016/j.colsurfa.2024.134321.